

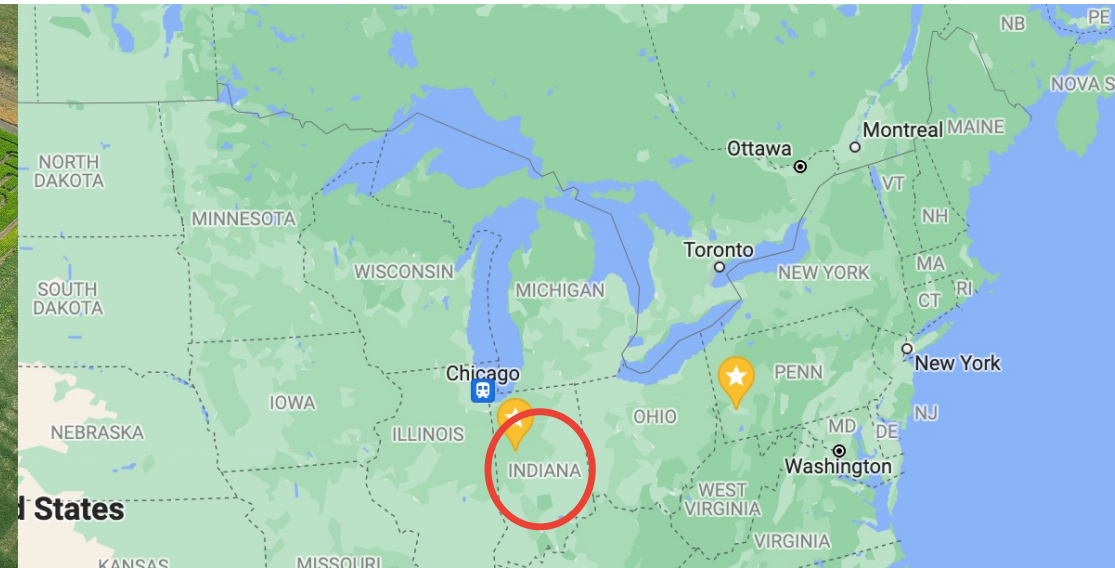


What do you want to be?

Could we bring values to others?

# Lesson 2

# Build Deep Expertise



[https://www.purdueexponent.org/campus/article\\_f2cf5c50-b3b0-11e9-82ce-f393b3730296.html](https://www.purdueexponent.org/campus/article_f2cf5c50-b3b0-11e9-82ce-f393b3730296.html)



Google Map

[https://www.dreamstime.com/statue-neil-armstrong-campus-purdue-university-west-lafayette-january-nasa-astronomer-sits-outside-hall-image172662206#\\_](https://www.dreamstime.com/statue-neil-armstrong-campus-purdue-university-west-lafayette-january-nasa-astronomer-sits-outside-hall-image172662206#_)



<https://www.tmahlmann.com/2017/04/spring-color-is-back-at-purdue/>



<https://www.purdue.edu/newsroom/releases/2020/Q3/expert-tech-that-could-reduce-summer-road-construction.html>



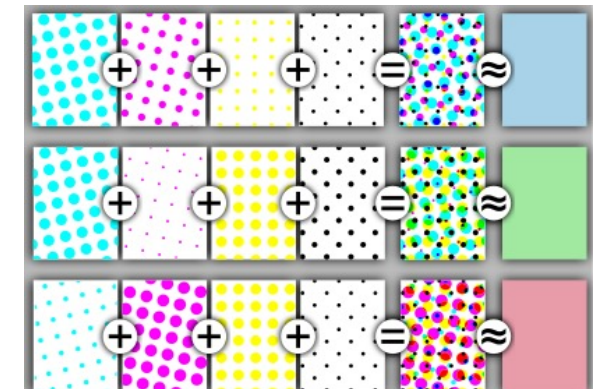
<https://www.tmahlmann.com/2017/01/a-beautiful-fall-afternoon-at-purdue/>



<https://twitter.com/LifeAtPurdue/status/1360227331210641409/photo/2>

# Research at Purdue

- I found my research funding in my second semester
  - Prof. Jan Allebach
  - Digital Imaging (halftoning)



Halftone

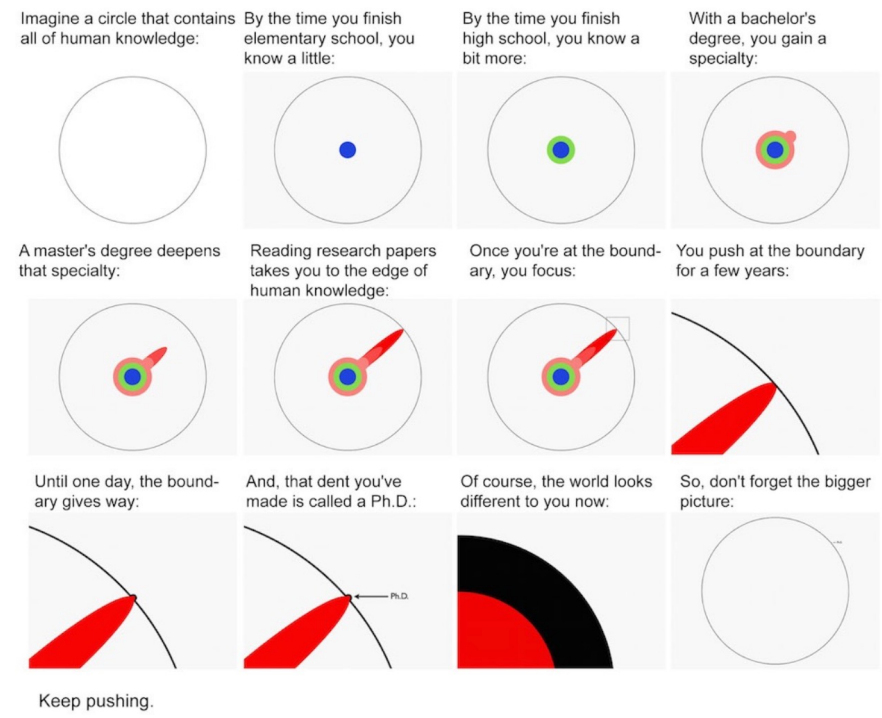
# My Thesis

- Composed of 3 **independent** projects

- Unsatisfactory
- Why: limited knowledge advancement

- Why?

- Partly because of funding sources
- Partly because of my intention...



<https://www.openculture.com/2017/06/the-illustrated-guide-to-a-phd-12-simple-pictures-that-will-put-the-daunting-degree-into-perspective.html>

# A Frustrating Job Interview

你做事情滿快的，可以很快完成不同的projects

但是...

你學問做得不深！

I know what he meant

I don't know how I should respond...

# Takeaway

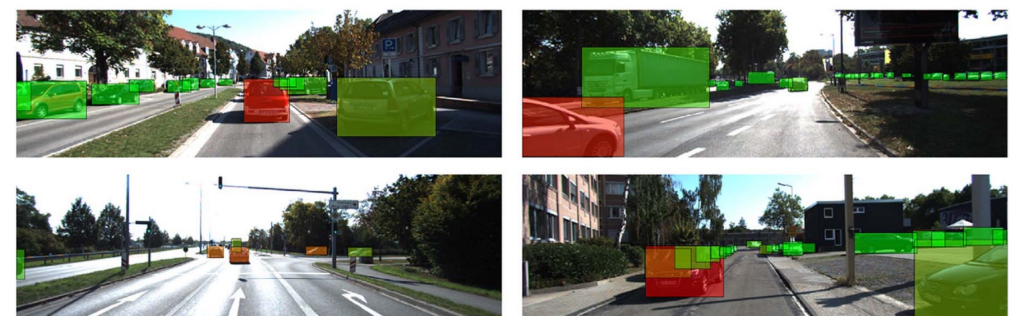
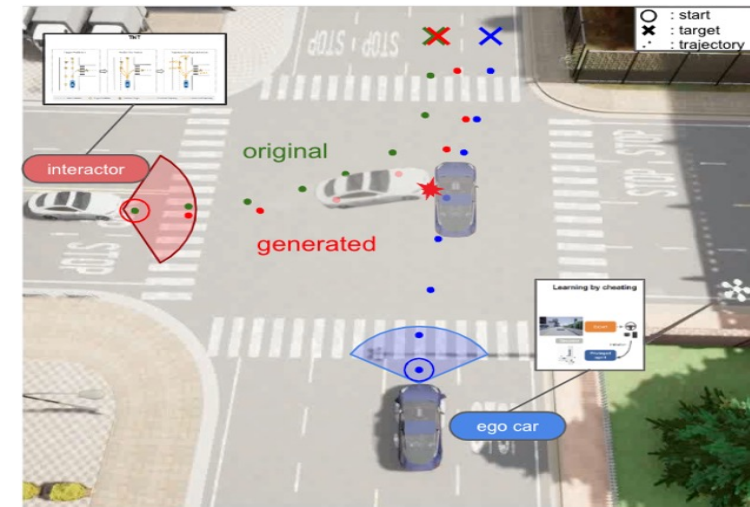
- We do lots of projects because of courses or 專題
  - We often stop thinking about them after submission
- If you found some projects/topics that you are interested in,

Go Deeper!

讓它變成可以侃侃而談的主題

# Important Object Identification

- **Objective**
  - Estimate collision risks/probability
    - Rule-based
    - Trajectory prediction and collision checking
    - Accident detection and anticipation
- **Subjective**
  - Output of human's cognitive process
    - Object importance
    - Driver gaze prediction
    - Driver behavior change

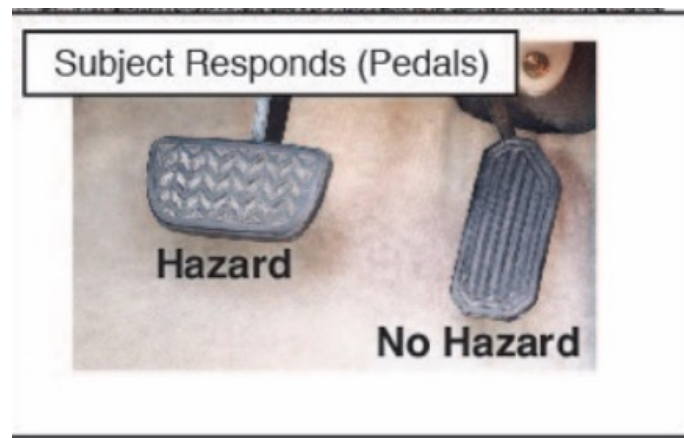


<https://eshed1.github.io/papers/areall.pdf>

# Human Risk Perception

What is the computational model of human risk perception?

- Based on a study reported in Wolfe et al., humans (388 msec younger; 605 msec older) can respond (hit brake pedal) correctly



Wolfe et al., Rapid Holistic Perception and Evasion of Road Hazards, Journal of Experimental Psychology: General (2019)

# Ongoing Efforts of my Exploration

- Chi-Hsi Kung, Chieh-Chi Yang, Pang-Yuan Pao, Shu-Wei Lu, Pin-Lun Chen, Hsin-Cheng Lu, Yi-Ting Chen, RiskBench: A Scenario-based Risk Identification Benchmark, IEEE Conference on Robotics and Automation (ICRA), 2024.
- Chi-Hsi Kung, Shu-Wei Lu, Yi-Hsuan Tsai, Yi-Ting Chen, Action-Slot: Visual Action-centric Representation for Traffic Pattern Recognition, IEEE Conference on Computer Vision and Pattern Recognition (CVPR), 2024
- C. Li, S. H. Chan, Y.-T. Chen, "DROID: Driver-centric Risk Object Identification, IEEE Transactions on Pattern Analysis and Machine Intelligence (T-PAMI), Volume: 45, [Issue: 11](#), 01, November, 2023.
- Z. Xiao, A. Yuille, Y.-T. Chen, "Learning Road Scene-level Representations via Semantic Region Prediction," Conference on Robot Learning (CoRL), 2022.
- N. Agarwal, Y.-T. Chen, "Towards Driver Behavior Understanding: Risk Perception in Driving Scenes," NeurIPS ML4AD workshop, 2022.
- I. Dwivedi, S. Malla, Y.-T. Chen, and B. Dariush, "Bird's Eye View Segmentation Using Lifted 2D Semantic Features," British Machine Vision Conference (BMVC), 2021.
- C. Li, Stanley H. Chan, and Y.-T. Chen, Who Make Drivers Stop? Towards Driver-centric Risk Assessment: Risk Object Identification via Causal Inference, IEEE International Conference on Intelligent Robots and Systems (IROS), 2020.
- M. Xu\*, M. Gao\*, Y.-T. Chen, L. Davis, and D. Crandall, "Temporal Recurrent Networks for Online Action Detection," IEEE International Conference on Computer Vision (ICCV), 2019.
- V. Ramanishka, Y.-T. Chen, T. Misu, and K. Saenko, "Toward Driving Scene Understanding: A Dataset for Learning Driver Behavior and Causal Reasoning," IEEE Conference on Computer Vision and Pattern Recognition (CVPR), 2018.

# Instrumented Vehicle

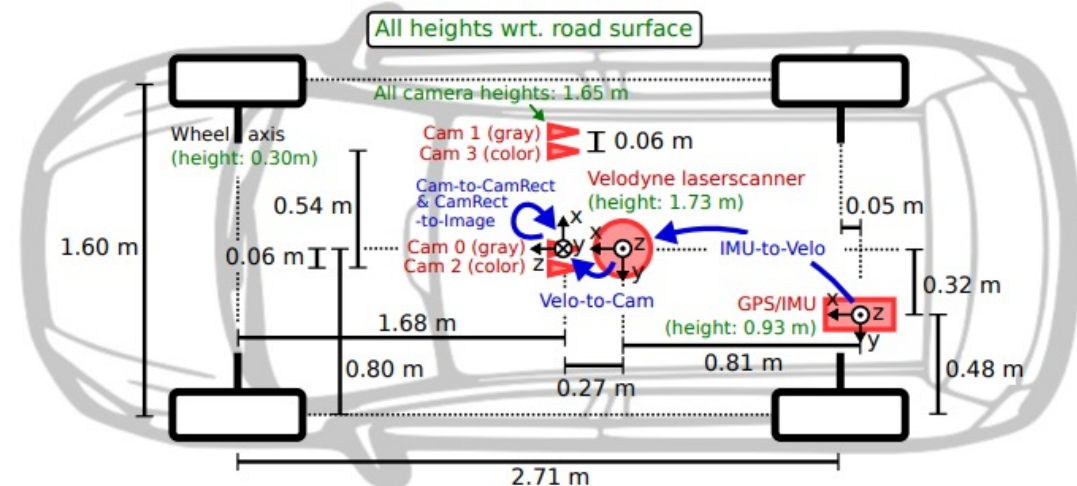
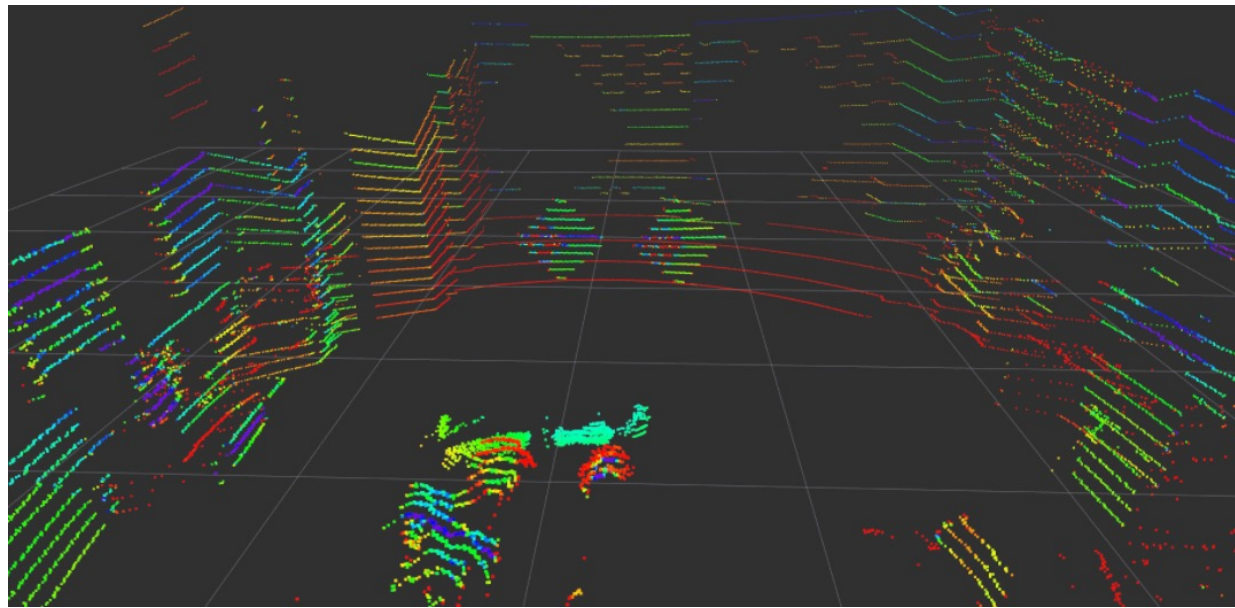
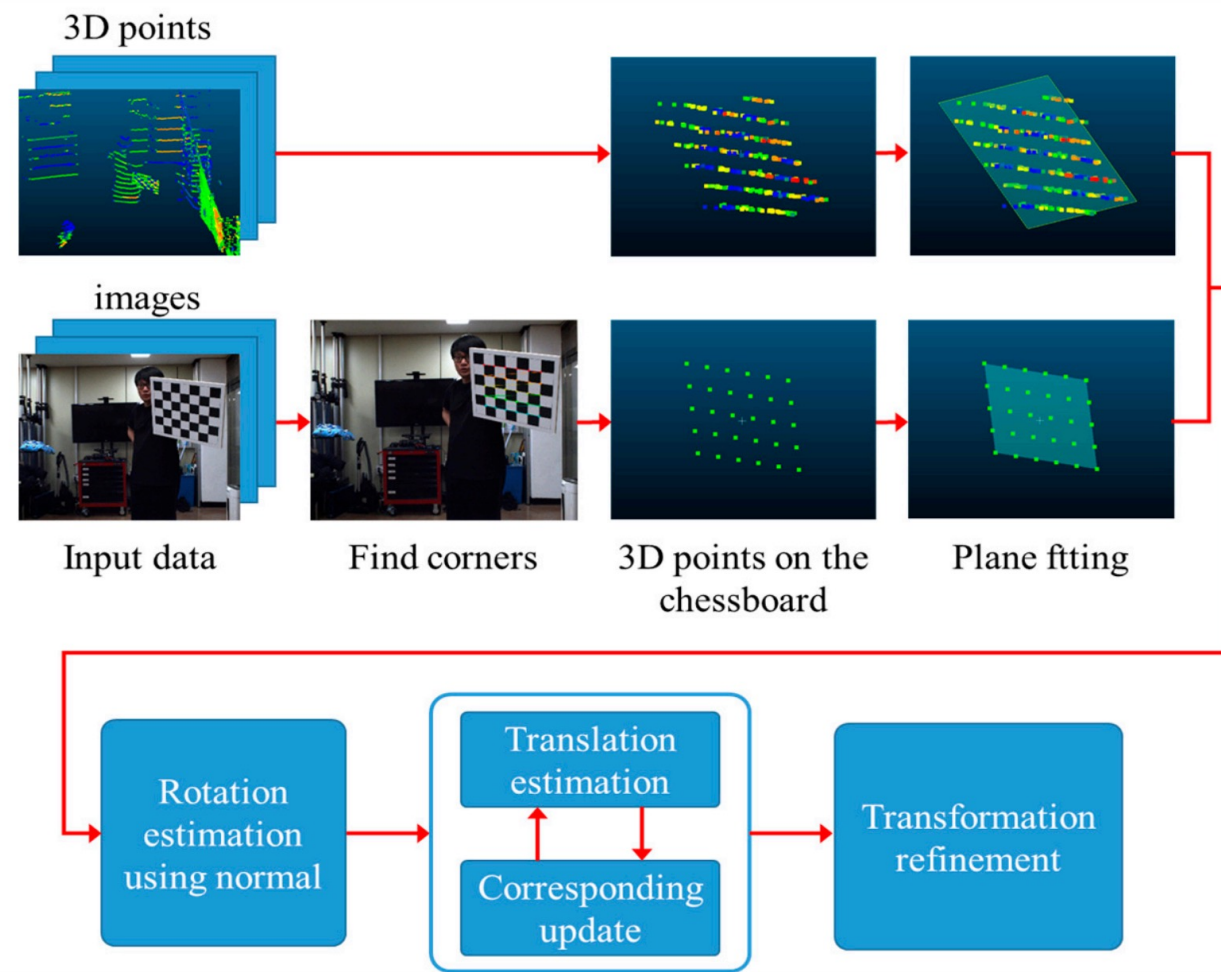


Fig. 3. **Sensor Setup.** This figure illustrates the dimensions and mounting positions of the sensors (red) with respect to the vehicle body. Heights above ground are marked in green and measured with respect to the road surface. Transformations between sensors are shown in blue.



<https://www.arxiv-vanity.com/papers/1705.09785/>



<https://www.mdpi.com/1424-8220/20/1/52/htm>



Credit: Google Map

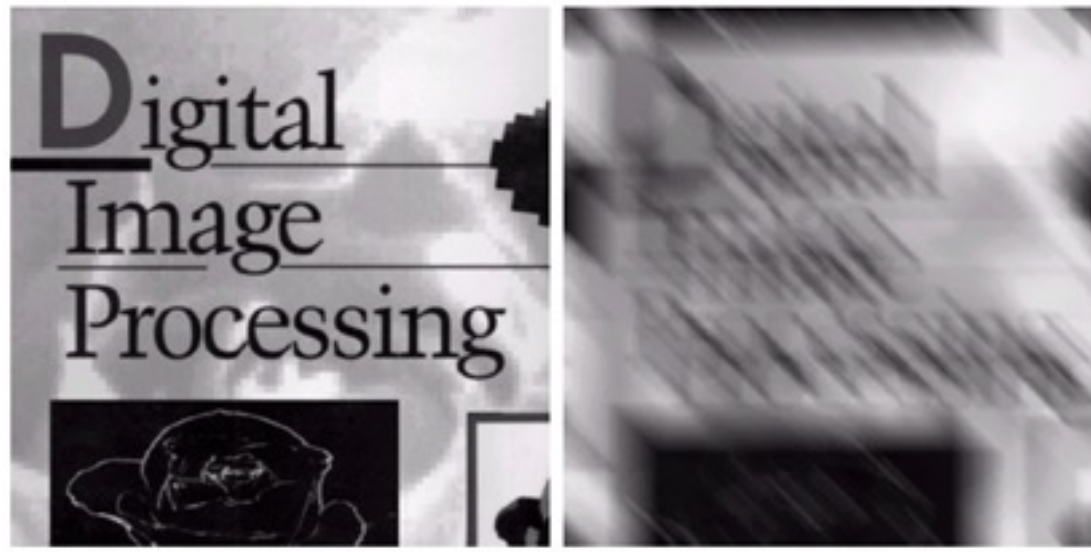


# Image Restoration

Fall 2024

Yi-Ting Chen

# Background

- Recover an image that has been degraded by using a priori knowledge of the degradation phenomenon.  
Key: (1) Estimate the degradation process (model) implicitly or explicitly  
(2) Design the inverse process (of the degradation)

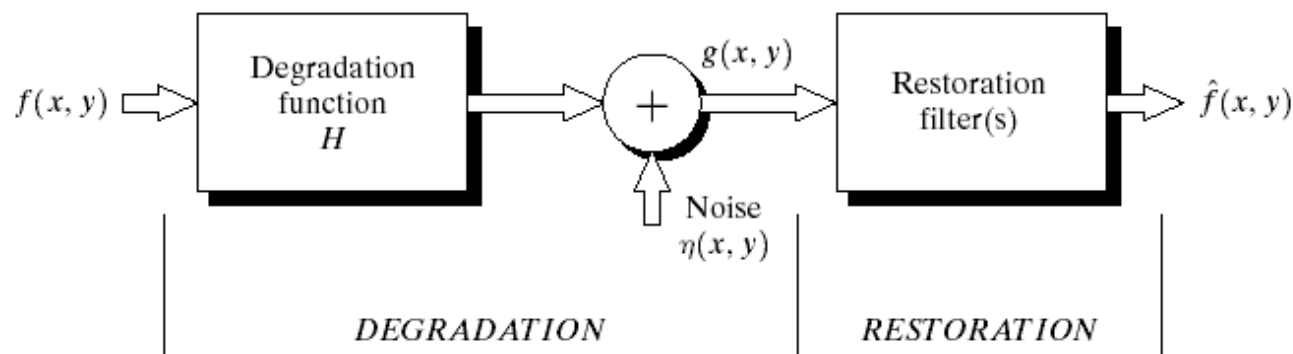
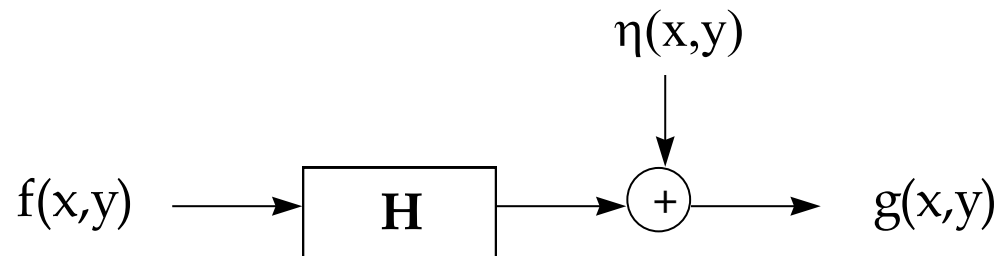


**FIGURE 5.1** A model of the image degradation/ restoration process.

- Many types of degradation can be approximated by linear, position-invariant processes.

$$\text{Spatial Domain: } g(x, y) = h(x, y) * f(x, y) + \eta(x, y)$$

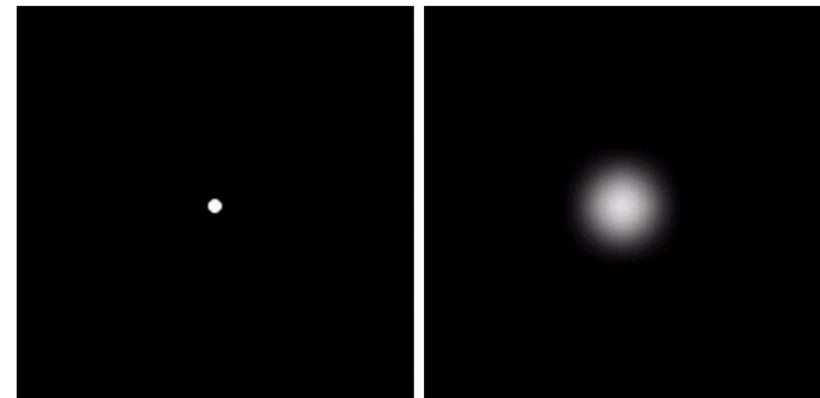
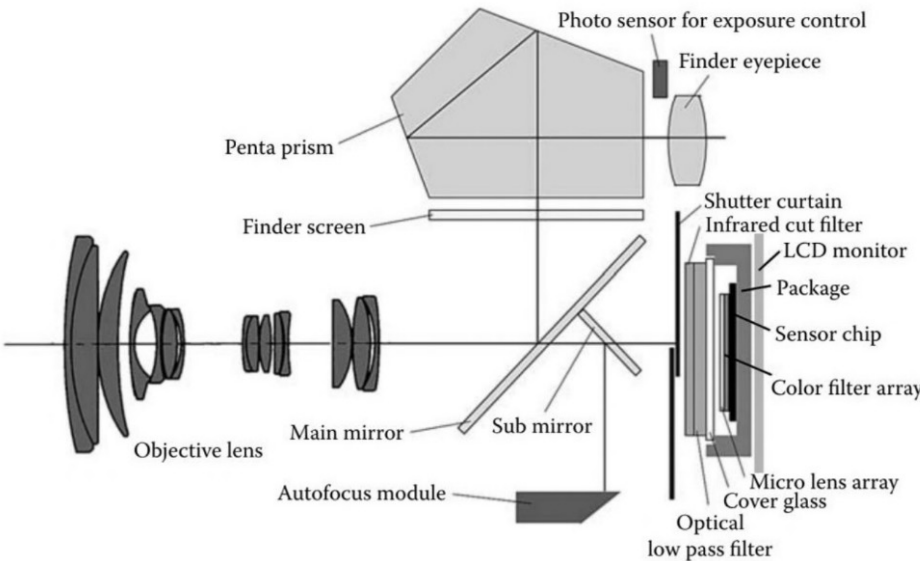
$$\text{Frequency Domain: } G(u, v) = H(u, v)F(u, v) + N(u, v)$$



$$g(x, y) = \int_{-\infty}^{\infty} \int_{-\infty}^{\infty} f(\alpha, \beta)h(x - \alpha, y - \beta)d\alpha d\beta + \eta(x, y)$$

Restoration: given  $g(x, y)$  and  $H$ , try to recover  $f(x, y)$ .

# Imaging System Degradation



a b

**FIGURE 5.24**  
Degradation estimation by impulse characterization.  
(a) An impulse of light (shown magnified).  
(b) Imaged (degraded) impulse.



High Quality Lens

Low Quality Lens

To reduce chromatic and other kinds of aberrations, most photographic lenses are compound lenses made of different glass elements (with different coatings)

# Imaging Degradation



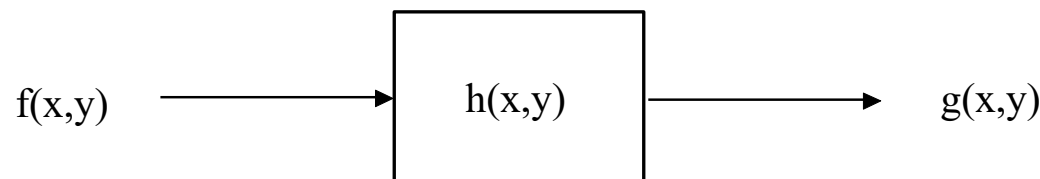
# Estimating the Degradation Function (1/6)

- **Estimation by Image Observation**

identify the degradation function from the image: points, lines, edges ...

$$H_s(u,v) = \frac{G_s(u,v)}{\hat{F}_s(u,v)}$$

- **Estimation by Experimentation**



$$H(u,v) = \frac{G(u,v)}{F(u,v)}$$

## Estimating the Degradation Function (2/6)

point source targets  $g(x,y) = \text{PSF}$

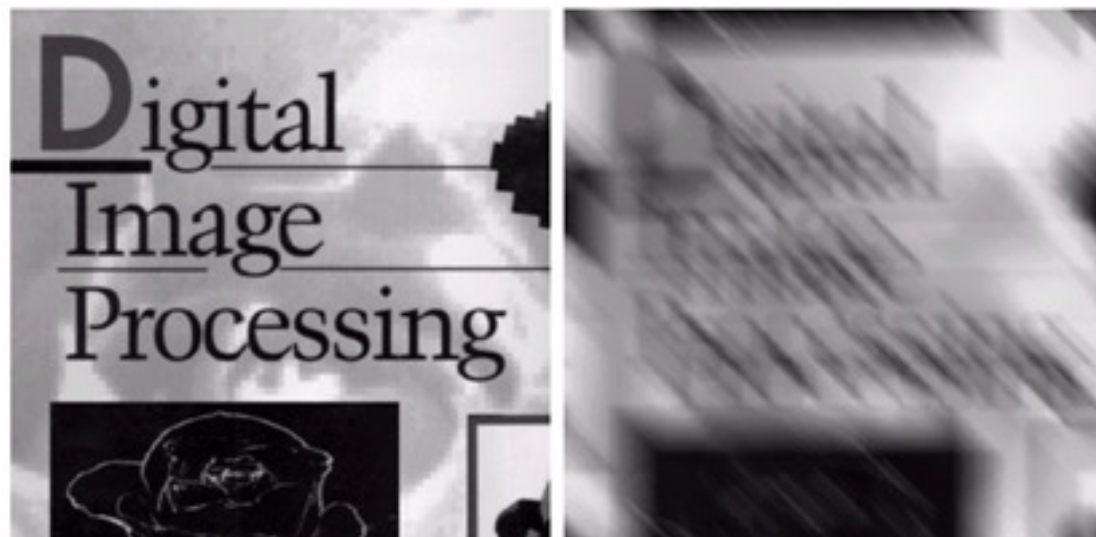
sine wave targets  $f(x,y) = \cos(2\pi s_0 x) \Rightarrow g(x,y) = H(s_0,0) \cos(2\pi s_0 x)$

line targets  $f(x,y) = \delta(x) \Rightarrow g(x,y) = \int_{-\infty}^{\infty} h(x,y) dy$   
 $\Rightarrow G(u,v) = H(u,0) \delta(v)$

edge targets  $f(x,y) = u(x) \Rightarrow G(u,v) = \frac{H(u,0)\delta(v)}{j2\pi u}$

or differentiate the edge-spread function

# Estimating the Degradation Function



a b

**FIGURE 5.26** (a) Original image. (b) Result of blurring using the function in Eq. (5.6-11) with  $a = b = 0.1$  and  $T = 1$ .

# Estimating the Degradation Function (4/6)

## Example: Uniform Linear Motion

Assume an image has been blurred by uniform linear motion between the image and the sensor during image acquisition.

$$g(x, y) = \int_0^T f[x - x_0(t), y - y_0(t)] dt$$

$$\begin{aligned} G(u, v) &= \int_{-\infty}^{\infty} \int_{-\infty}^{\infty} g(x, y) e^{-j2\pi(ux+vy)} dx dy \\ &= \int_{-\infty}^{\infty} \int_{-\infty}^{\infty} \left[ \int_0^T f[x - x_0(t), y - y_0(t)] dt \right] e^{-j2\pi(ux+vy)} dx dy \\ G(u, v) &= \int_0^T \left[ \int_{-\infty}^{\infty} \int_{-\infty}^{\infty} f[x - x_0(t), y - y_0(t)] e^{-j2\pi(ux+vy)} dx dy \right] dt \end{aligned}$$

# Estimating the Degradation Function (6/6)

$$G(u, v) = \int_0^T F(u, v) e^{-j2\pi[ux_0(t)+vy_0(t)]} dt = F(u, v) \int_0^T e^{-j2\pi[ux_0(t)+vy_0(t)]} dt$$

Define

$$\text{Then, } G(u, v) = H(u, v)F(u, v)$$

Suppose the image undergoes uniform linear motion in the x-direction only.

$$H(u, v) = \int_0^T e^{-j2\pi ux_0(t)} dt = \int_0^T e^{-j2\pi uat/T} dt = \frac{T}{\pi ua} \sin(\pi ua) e^{-j\pi ua}$$

Suppose  $x_0(t) = at/T$  and  $y_0(t) = bt/T$

$$H(u, v) = \frac{T}{\pi(ua + vb)} \sin[\pi(ua + vb)] e^{-j\pi(ua + vb)}$$

# Laser Scanner Jitter

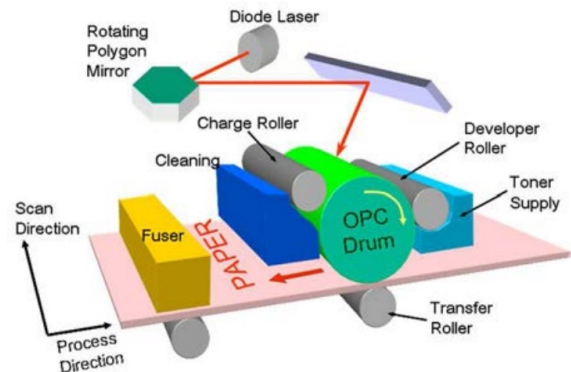
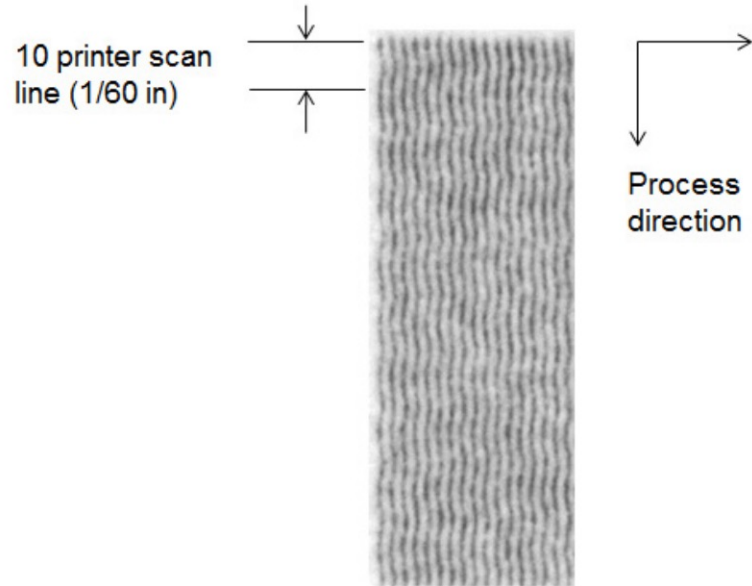


Fig. 1.1. Architecture of a typical electrophotographic printer. [1]



**Figure 1.** Straight lines printed in the process direction appear to be wiggly instead of straight. The length of each straight line is 100 printer-addressable pixels, and the periodic pattern repeats every 10 pixels because the polygon mirror in our target laser printer has 10 facets. The printer resolution is 600 dpi.

# Mathematical Modeling

## Mathematical Model of Laser Scanner Jitter

We first develop the general mathematical model of periodic laser scanner jitter in a two-dimensional continuous-space for a continuous-tone image, and extend it to the special case of a sinusoidal displacement in the next section. We denote the continuous-tone image by  $f(x, y)$ . Here  $x$  corresponds to the process (vertical) direction, and  $y$  corresponds to the scan (horizontal) direction. We define a new image  $g(x, y)$ , with periodic laser scanner jitter, according to

$$g(x, y) = f(x, y - d(x)), \quad (1)$$

where the displacement  $d(x)$  is periodic in  $x$ . Let  $F(u, v)$  denote the two-dimensional Continuous-Space Fourier Transform

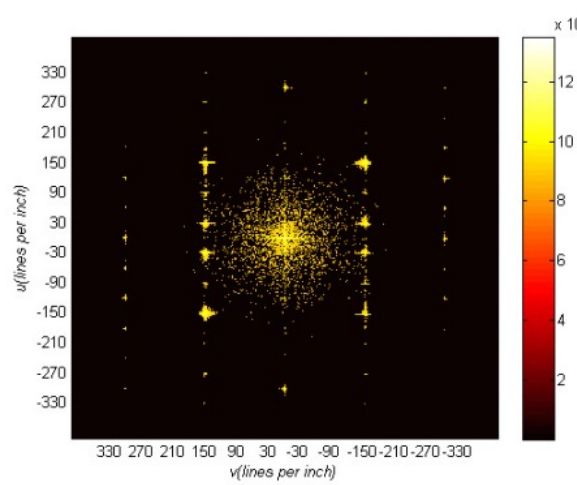
### Periodic Laser Scanner Jitter with Sinusoidal Displacement

In this section, we extend the model to the special case where the periodic displacement is a sinusoid function  $d(x) = A \sin(2\pi x/X)$ . Here  $A$  is a constant scale factor that is the peak jitter displacement, and  $X$  is the period of the laser scanner jitter. With an approach similar to that used in the previous section, we

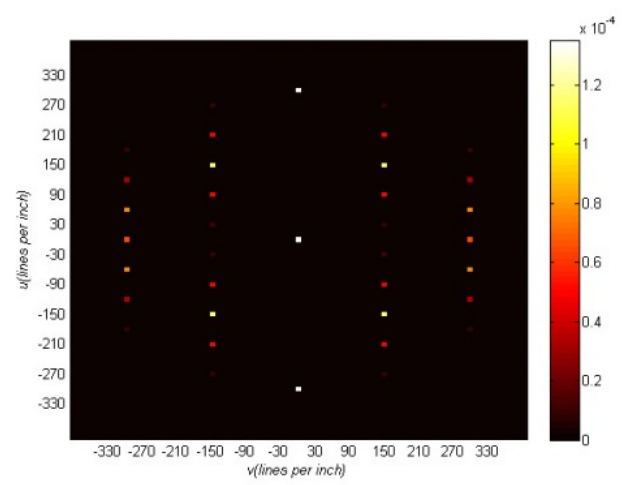
# Quantitative Experiments



(a)



(a)

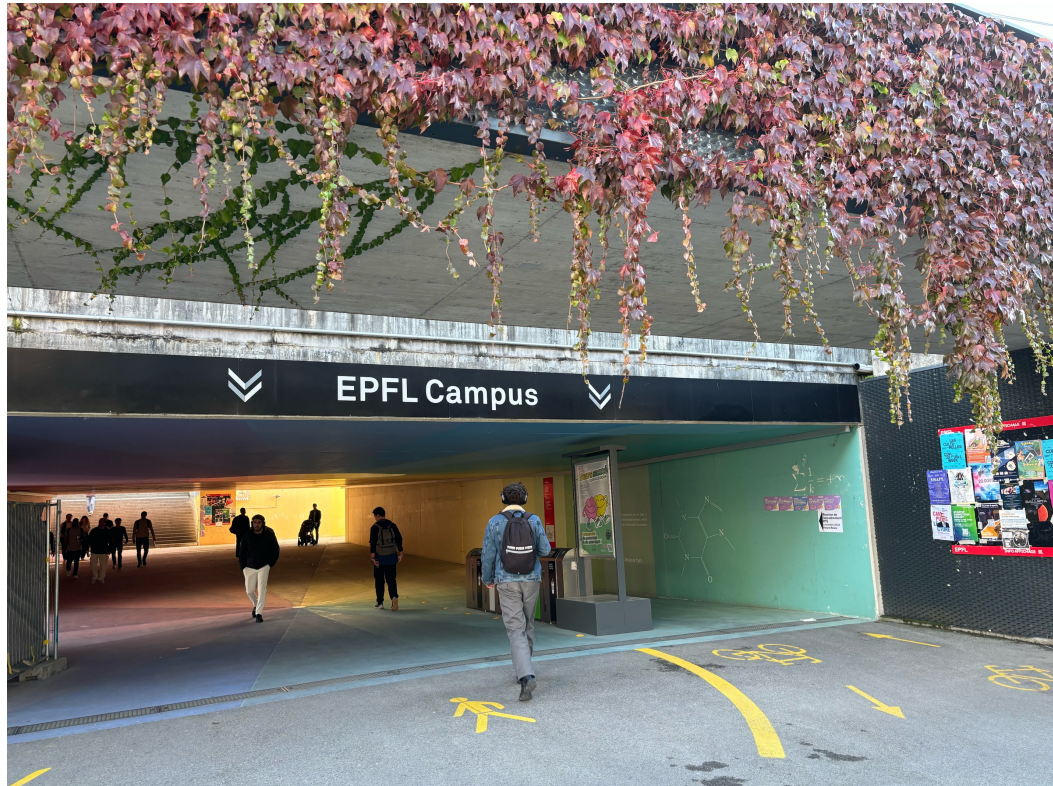


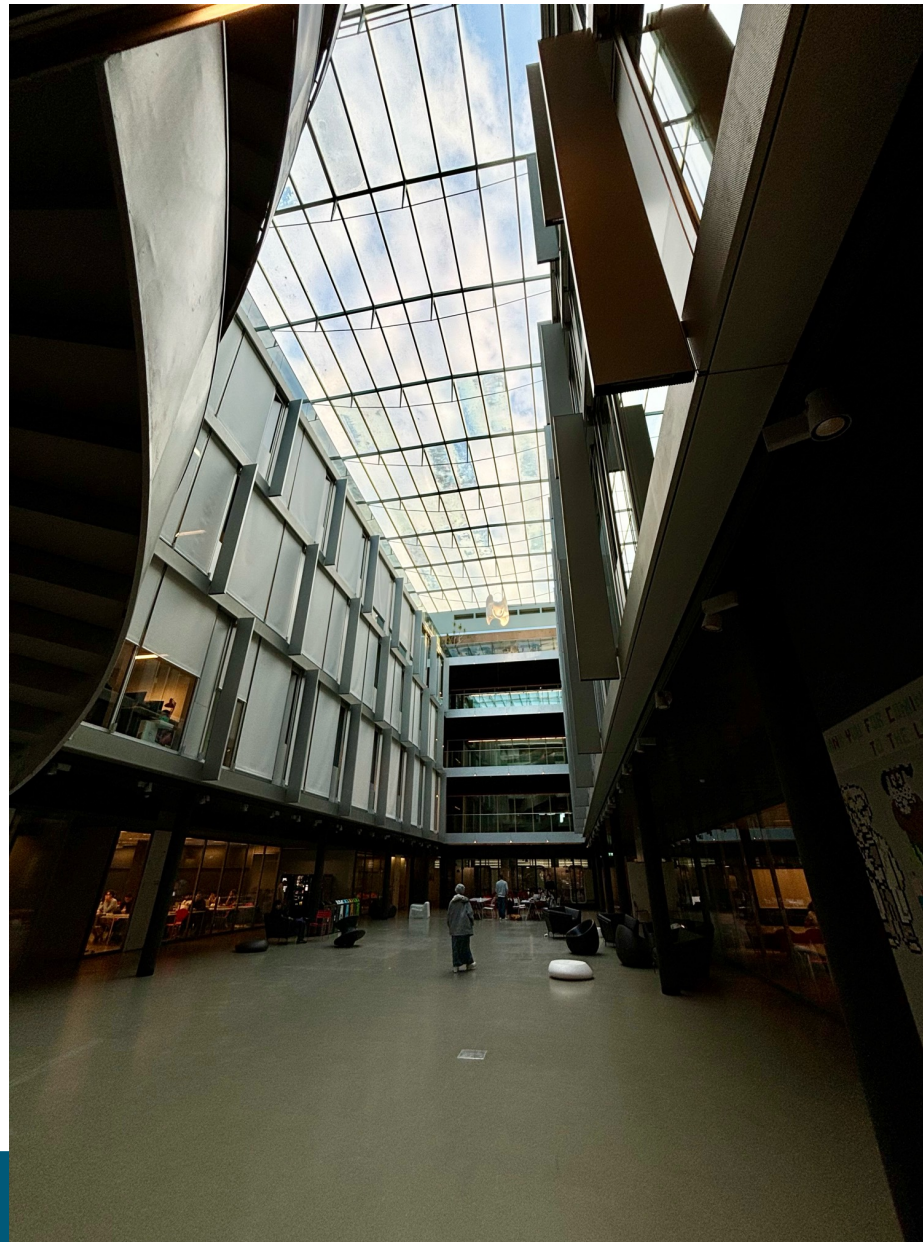
(b)

Science is what we understand well  
enough to explain to a computer.

Art is everything else we do.

# Swiss Federal Institute of Technology Lausanne



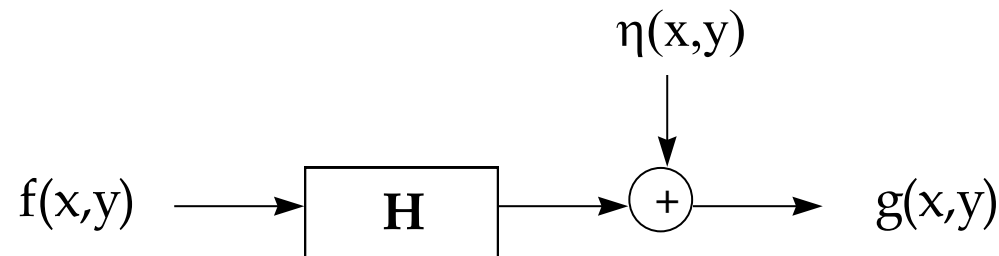


# **Restoration Methods**

# Image Restoration

$$\text{Spatial Domain: } g(x, y) = h(x, y) * f(x, y) + \eta(x, y)$$

$$\text{Frequency Domain: } G(u, v) = H(u, v)F(u, v) + N(u, v)$$



Restoration: given  $g(x, y)$  and  $H$ , try to recover  $f(x, y)$ .

# Inverse Filtering

$$\hat{F}(u, v) = \frac{G(u, v)}{H(u, v)}$$

$$\hat{F}(u, v) = F(u, v) + \frac{N(u, v)}{H(u, v)}$$

⇒ may cause problem for small H(u,v)

Issues: Need to know H(u,v) in advance.

H(u,v) cannot be close to zero for all (u,v)

Compute G(u,v)/H(u,v) only at low frequencies (u,v)

**Example:**  $H(u, v) = e^{-k[(u-M/2)^2 + (v-N/2)^2]^{5/6}}$

a b  
c d

**FIGURE 5.27**  
Restoring  
Fig. 5.25(b) with  
Eq. (5.7-1).  
(a) Result of  
using the full  
filter. (b) Result  
with  $H$  cut off  
outside a radius of  
40; (c) outside a  
radius of 70; and  
(d) outside a  
radius of 85.



# Minimum Mean Square Error (Wiener) Filtering

$$e^2 = E\{(f - \hat{f})^2\}$$

$$\begin{aligned}\hat{F}(u, v) &= \left[ \frac{H^*(u, v)S_f(u, v)}{S_f(u, v)|H(u, v)|^2 + S_\eta(u, v)} \right] G(u, v) \\ &= \left[ \frac{H^*(u, v)}{|H(u, v)|^2 + S_\eta(u, v)/S_f(u, v)} \right] G(u, v) \\ &= \left[ \frac{1}{H(u, v)} \frac{|H(u, v)|^2}{|H(u, v)|^2 + S_\eta(u, v)/S_f(u, v)} \right] G(u, v) \\ \hat{F}(u, v) &= \left[ \frac{1}{H(u, v)} \frac{|H(u, v)|^2}{|H(u, v)|^2 + K} \right] G(u, v)\end{aligned}$$

### Remark: **Geometric Mean Filter**

$$\hat{F}(u, v) = \left[ \frac{H^*(u, v)}{|H(u, v)|^2} \right]^\alpha \left[ \frac{H^*(u, v)}{|H(u, v)|^2 + \beta \left[ \frac{S_\eta(u, v)}{S_f(u, v)} \right]} \right]^{1-\alpha} G(u, v)$$

$\alpha = 1 \Rightarrow$  inverse filter

$\alpha = 0 \Rightarrow$  parametric Wiener filter

$\alpha = 0 \ \beta = 1 \Rightarrow$  standard Wiener filter

$\alpha = 1/2 \ \beta = 1 \Rightarrow$  spectrum equalization filter



a b c

**FIGURE 5.28** Comparison of inverse- and Wiener filtering. (a) Result of full inverse filtering of Fig. 5.25(b). (b) Radially limited inverse filter result. (c) Wiener filter result.

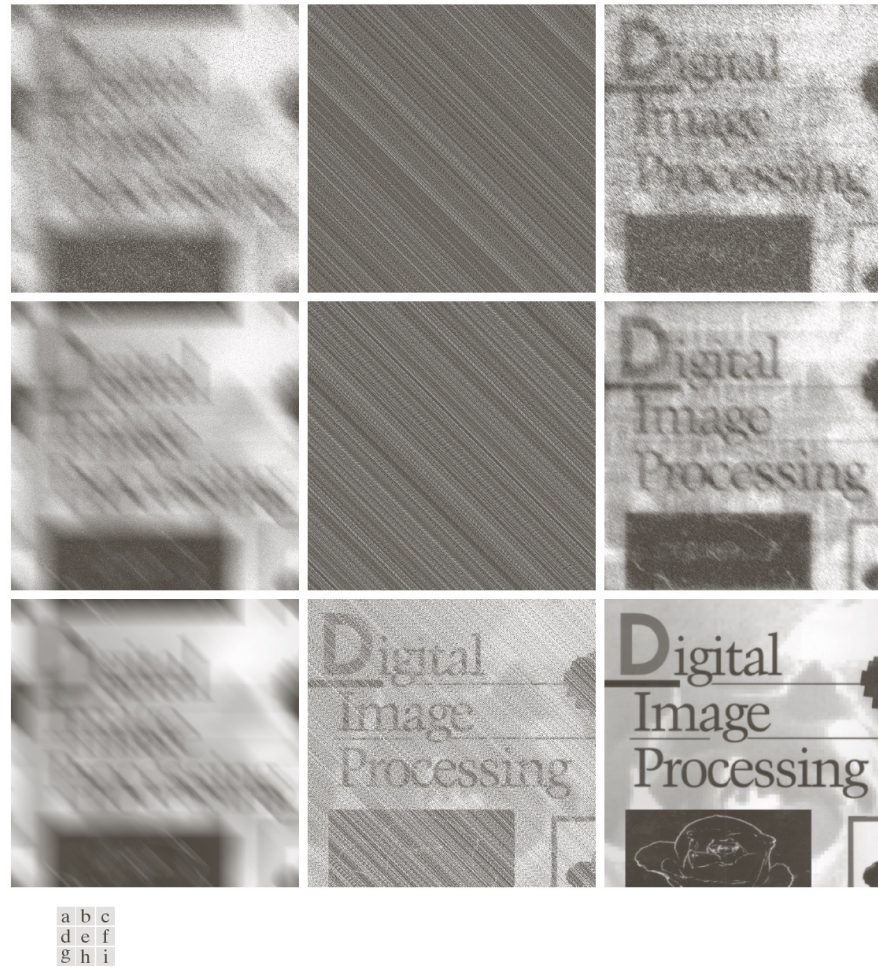


**FIGURE 5.29** (a) 8-bit image corrupted by motion blur and additive noise. (b) Result of inverse filtering. (c) Result of Wiener filtering. (d)–(f) Same sequence, but with noise variance one order of magnitude less. (g)–(i) Same sequence, but noise variance reduced by five orders of magnitude from (a). Note in (h) how the deblurred image is quite visible through a “curtain” of noise.

# Constrained Least Squares Restoration

$$\mathbf{g} = \mathbf{Hf} + \boldsymbol{\eta}$$

To base optimality of restoration on a measure of smoothness:  
⇒ Find the minimum of a criterion function C

$$C = \sum_{x=0}^{M-1} \sum_{y=0}^{N-1} [\nabla^2 \hat{f}(x, y)]^2$$

subject to the constraint  $\|\mathbf{g} - \mathbf{H}\hat{\mathbf{f}}\|^2 = \|\boldsymbol{\eta}\|^2$

$$\Rightarrow \hat{F}(u,v) = \left[ \frac{H^*(u,v)}{|H(u,v)|^2 + \gamma |P(u,v)|^2} \right] G(u,v)$$

where  $P(u,v)$  is the Fourier transform of  $p(x,y) = \begin{bmatrix} 0 & -1 & 0 \\ -1 & 4 & -1 \\ 0 & -1 & 0 \end{bmatrix}$

and  $\gamma$  is a parameter that must be adjusted so that the constraint is satisfied.



**FIGURE 5.30** Results of constrained least squares filtering. Compare (a), (b), and (c) with the Wiener filtering results in Figs. 5.29(c), (f), and (i), respectively.

## A procedure for computing $\gamma$ by iteration:

Define  $\mathbf{r} = \mathbf{g} - \mathbf{H}\hat{\mathbf{f}}$

It can be shown that

$\phi(\gamma) = \mathbf{r}^T \mathbf{r} = \|\mathbf{r}\|^2$  is a monotonically increasing function of  $\gamma$

What we want to do is adjust gamma so that  $\|\mathbf{r}\|^2 = \|\mathbf{n}\|^2 \pm a$

where  $a$  is an accuracy factor.

Step 1. Specify an initial value of  $\gamma$ .

Step 2. Compute  $\|\mathbf{r}\|^2$

Step 3. Stop if  $\|\mathbf{r}\|^2 = \|\mathbf{n}\|^2 \pm a$  is satisfied;

otherwise, return to Step 2 after increasing  $\gamma$  if  $\|\mathbf{r}\|^2 < \|\mathbf{n}\|^2 - a$   
or decreasing  $\gamma$  if  $\|\mathbf{r}\|^2 > \|\mathbf{n}\|^2 + a$

Use the new value of  $\gamma$  to recomputed the optimum estimate  $\hat{F}(u, v)$

- To compute  $\|\mathbf{r}\|^2$

$$R(u, v) = G(u, v) - H(u, v)\hat{F}(u, v)$$

$$\|\mathbf{r}\|^2 = \sum_{x=0}^{M-1} \sum_{y=0}^{N-1} r^2(x, y)$$

- To compute  $\|\boldsymbol{\eta}\|^2$

$$\sigma_\eta^2 = \frac{1}{MN} \sum_{x=0}^{M-1} \sum_{y=0}^{N-1} [\eta(x, y) - m_\eta]^2$$

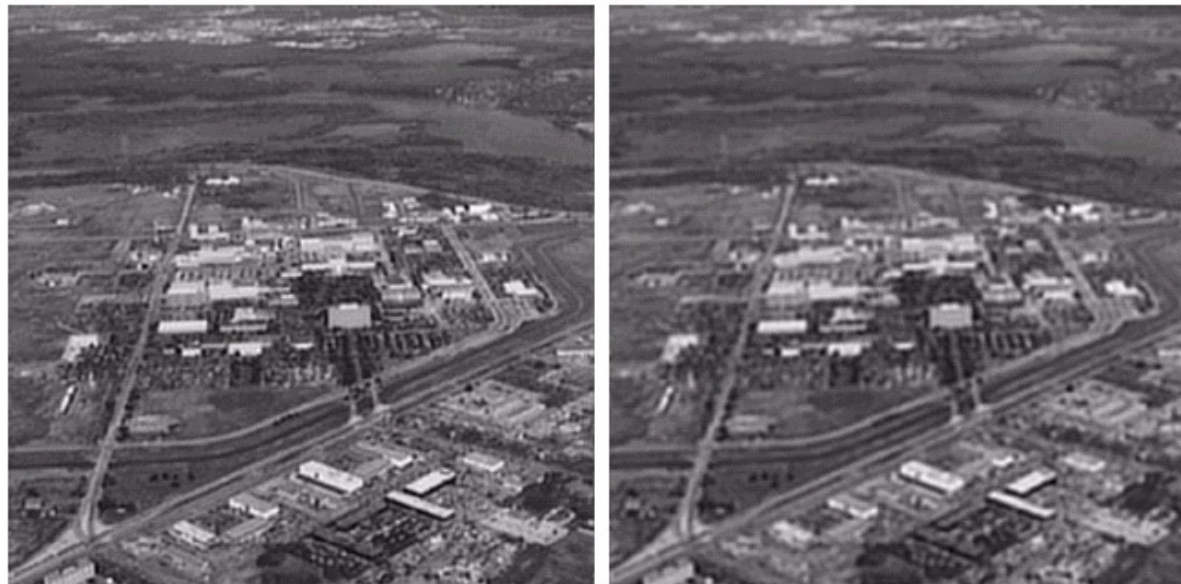
$$\Rightarrow \|\boldsymbol{\eta}\|^2 = MN[\sigma_\eta^2 + m_\eta^2]$$

where  $m_\eta = \frac{1}{MN} \sum_{x=0}^{M-1} \sum_{y=0}^{N-1} \eta(x, y)$

a b

**FIGURE 5.31**

(a) Iteratively determined constrained least squares restoration of Fig. 5.16(b), using correct noise parameters.  
(b) Result obtained with wrong noise parameters.



# **Blind Image Restoration**

# Blind Image Restoration

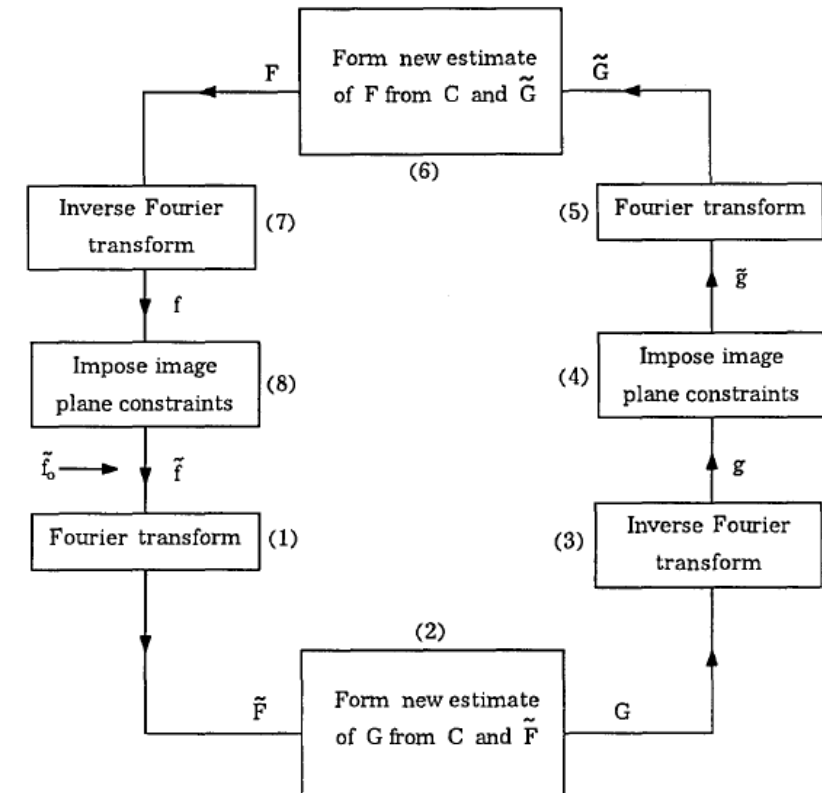
- Also named as “**Blind Image Deconvolution**”
- Both  $f(x, y)$  and  $h(x, y)$  are unknown
  - ⇒ There is an infinite set of pairs  $(f(x, y), h(x, y))$  that satisfy
$$g(x, y) = f(x, y) * h(x, y) + \eta(x, y).$$
  - ⇒ Additional assumptions on  $f(x, y)$  and  $h(x, y)$  must be introduced.

# Earlier Methods

$$c(\mathbf{x}, \mathbf{y}) = f(\mathbf{x}, \mathbf{y}) * g(\mathbf{x}, \mathbf{y})$$

Assumption:

- Nonnegativity on both  $f(\mathbf{x}, \mathbf{y})$  and  $g(\mathbf{x}, \mathbf{y})$



Ref: Ayers, G. R., and J. Christopher Dainty. "Iterative blind deconvolution method and its applications." Optics letters 13.7 (1988): 547-549.

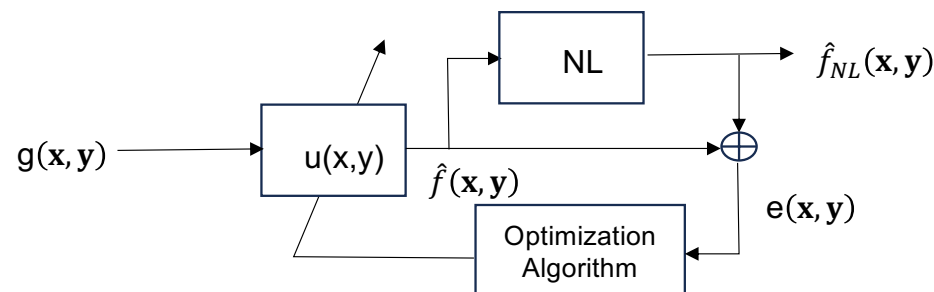
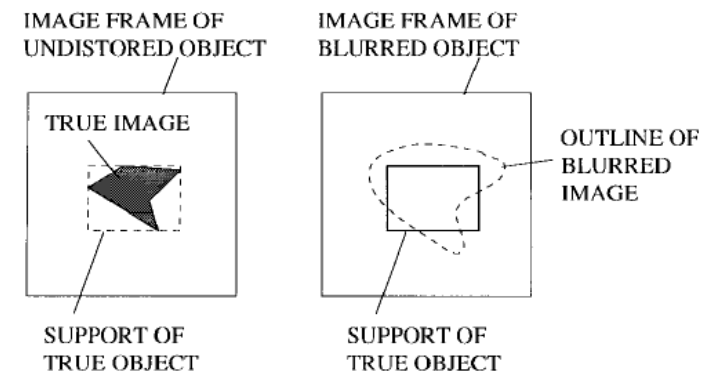
# Earlier Methods

## NAS-RIF

$$g(\mathbf{x}, \mathbf{y}) = f(\mathbf{x}, \mathbf{y}) * h(\mathbf{x}, \mathbf{y})$$

Assumption:

- Nonnegativity & Compact Support on  $f(\mathbf{x}, \mathbf{y})$
- $\sum_{\forall \mathbf{x}} |h(\mathbf{x}, \mathbf{y})| < \infty$  and  $\sum_{\forall \mathbf{x}} |h^{-1}(\mathbf{x}, \mathbf{y})| < \infty$



$$\hat{f}_{NL}(\mathbf{x}, \mathbf{y}) = \begin{cases} \hat{f}(\mathbf{x}, \mathbf{y}) & \text{if } \hat{f}(\mathbf{x}, \mathbf{y}) \geq 0 \text{ and } (\mathbf{x}, \mathbf{y}) \in D_{sup} \\ 0 & \text{if } \hat{f}(\mathbf{x}, \mathbf{y}) < 0 \text{ and } (\mathbf{x}, \mathbf{y}) \in D_{sup} \\ L_B & \text{if } (\mathbf{x}, \mathbf{y}) \notin D_{sup} \end{cases}$$

Ref: Kundur, Deepa, and Dimitrios Hatzinakos. "A novel blind deconvolution scheme for image restoration using recursive filtering." IEEE transactions on signal processing 46.2 (1998): 375-390.

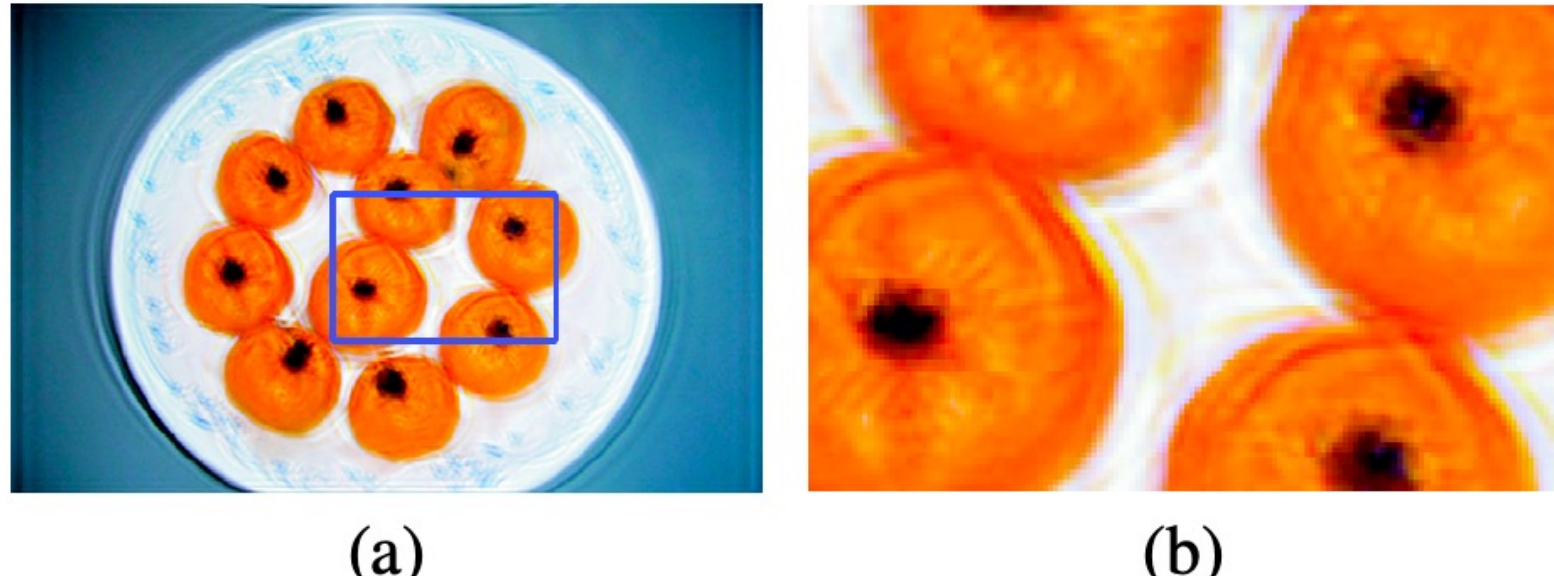


**Figure 2** Ringing artifacts in image deconvolution. (a) A blind deconvolution result. (b) A magnified patch from (a). Ringing artifacts are visible around strong edges.

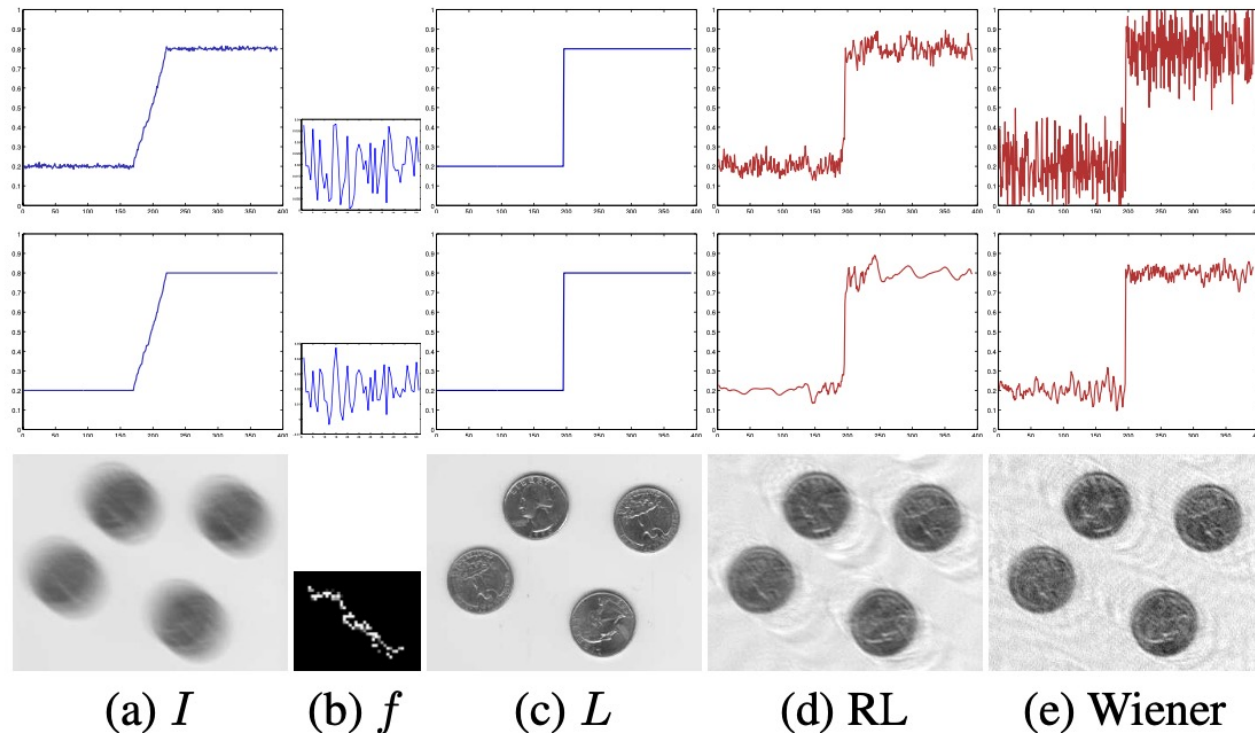


**Figure 4** Noise in deconvolution. The first two rows show 1D signal examples corrupted with signal noise and kernel noise, respectively. The last row shows an image example in the presence of both image noise and kernel noise. For all rows, (a) shows the observed signals. (b) The kernel. (c) The ground truth signal. (d) The reconstructed signal using RL method. (e) The reconstructed signal by Wiener filtering. Artifact can be seen in the deconvolution results.

To analyze the problems caused by image noise and kernel error, let us model the kernel and latent image as the sum of their current estimates  $\mathbf{f}'$  and  $\mathbf{L}'$  and the errors  $\Delta\mathbf{f}$  and  $\Delta\mathbf{L}$ :

$$\begin{aligned}\mathbf{I} &= (\mathbf{L}' + \Delta\mathbf{L}) \otimes (\mathbf{f}' + \Delta\mathbf{f}) + \mathbf{n} \\ &= \mathbf{L}' \otimes \mathbf{f}' + \Delta\mathbf{L} \otimes \mathbf{f}' + \mathbf{L}' \otimes \Delta\mathbf{f} + \Delta\mathbf{L} \otimes \Delta\mathbf{f} + \mathbf{n}.\end{aligned}$$

In the above equation, we can see that if observed noise  $\mathbf{n}$  is not modeled well, it is easy for an estimation algorithm to mistake errors  $\Delta\mathbf{f}$  and  $\Delta\mathbf{L}$  as part of the noise  $\mathbf{n}$ , making the estimation process unstable and challenging to solve. Previous techniques typically model image noise  $\mathbf{n}$  or its gradient  $\partial\mathbf{n}$  as following zero-mean Gaussian distributions. This model is weak and subject to the risk outlined above because it does not capture an important property of image noise, which is that image noise exhibits *spatial randomness*. To illustrate, in Figure 6(d) we show that replacing our stronger model of noise (described in the next section) with a simple zero-mean Gaussian yields a noise estimate  $(\mathbf{L} \otimes \mathbf{f} - \mathbf{I})$  that is clearly structured and not spatially random.



(a)



(b)

Blurred Image  
 $g(x,y)$

$\hat{f}(x,y)$  Based on  
Traditional Model



(c)

$g(x,y) - \hat{f}(x,y) * \hat{h}(x,y)$



(d)



(e)

$\hat{f}(x,y)$  Based on  
New Model

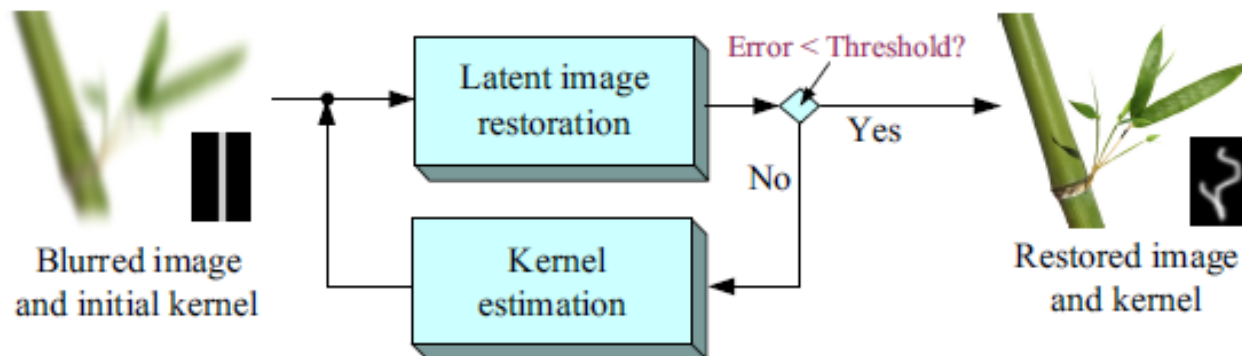


(f)

$g(x,y) - \hat{f}(x,y) * \hat{h}(x,y)$

# High-Quality Motion Deblurring from a Single Image

- Model the spatially random distribution of image noise
- Smoothness constraint over regions of low contrast
- Propose an efficient optimization algorithm



$$g(\mathbf{x}, \mathbf{y}) = f(\mathbf{x}, \mathbf{y}) * h(\mathbf{x}, \mathbf{y}) + n(\mathbf{x}, \mathbf{y})$$

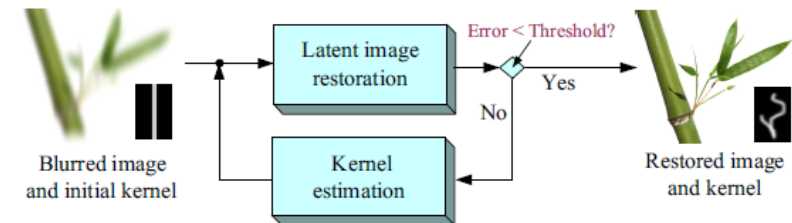
# MAP (Maximum a Posteriori)

- Formulation (A probabilistic model unifies blind and non-blind restoration)

$$g(x, y) = f(x, y) * h(x, y) + n(x, y)$$

$$p(f, h | g) \propto p(g | f, h) p(f) p(h)$$

$p(f, h   g)$	Posterior probability function
$p(g   f, h)$	Likelihood model
$p(f)$	prior probability on latent image
$p(h)$	prior probability on the blur kernel



# Likelihood Model

$$p(g|f, h) \quad \text{Likelihood model} \quad g(\mathbf{x}, \mathbf{y}) - f(\mathbf{x}, \mathbf{y}) * h(\mathbf{x}, \mathbf{y}) = n(\mathbf{x}, \mathbf{y})$$

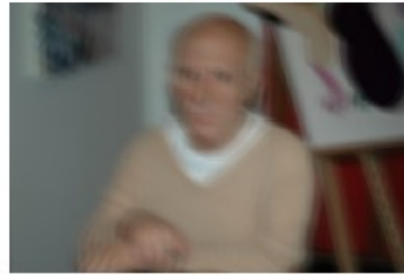
- Typically, the likelihood term is written as
  - ✓  $[g(\mathbf{x}, \mathbf{y}) - f(\mathbf{x}, \mathbf{y}) * h(\mathbf{x}, \mathbf{y})] \sim N(0, \zeta_0)$
  - ✓  $\frac{\partial(g(\mathbf{x}, \mathbf{y}) - f(\mathbf{x}, \mathbf{y}) * h(\mathbf{x}, \mathbf{y}))}{\partial \mathbf{x}} \sim N(0, \zeta_1)$
  - ✓  $\frac{\partial(g(\mathbf{x}, \mathbf{y}) - f(\mathbf{x}, \mathbf{y}) * h(\mathbf{x}, \mathbf{y}))}{\partial \mathbf{y}} \sim N(0, \zeta_1)$

If we compute the partial derivatives as  $\frac{\partial n(x, y)}{\partial x} = n(x + 1, y) - n(x, y)$  and  $\frac{\partial n(x, y)}{\partial y} = n(x, y + 1) - n(x, y)$ , then  $\zeta_1 = \sqrt{2}\zeta_0$ .

However, these low-order statistics do not capture the spatial randomness of noise.



(a)



(b)

Blurred Image  
 $g(x,y)$

$\hat{f}(x,y)$  Based on  
Traditional Model



(c)



(e)

$\hat{f}(x,y)$  Based on  
New Model

$g(x,y) - \hat{f}(x,y) * \hat{h}(x,y)$



(d)



(f)

$g(x,y) - \hat{f}(x,y) * \hat{h}(x,y)$

## Example 1 - Sum of two independent normal random variables

The sum of two independent normal random variables has a normal distribution.

**Proposition** Let  $X_1$  be a normal random variable with mean  $\mu_1$  and variance  $\sigma_1^2$ . Let  $X_2$  be a random variable, independent of  $X_1$ , having a normal distribution with mean  $\mu_2$  and variance  $\sigma_2^2$ . Then, the random variable

$$Y = X_1 + X_2$$

has a normal distribution with mean

$$\mathbb{E}[Y] = \mu_1 + \mu_2$$

and variance

$$\text{Var}[Y] = \sigma_1^2 + \sigma_2^2$$

# Likelihood Model

$p(g|f, h)$  Likelihood model

- New Model

$$\checkmark (g(\mathbf{x}, \mathbf{y}) - f(\mathbf{x}, \mathbf{y}) * h(\mathbf{x}, \mathbf{y})) \sim N(0, \zeta_0)$$

$$\checkmark \frac{\partial(g(\mathbf{x}, \mathbf{y}) - f(\mathbf{x}, \mathbf{y}) * h(\mathbf{x}, \mathbf{y}))}{\partial \mathbf{x}} \sim N(0, \zeta_1)$$

$$\checkmark \frac{\partial(g(\mathbf{x}, \mathbf{y}) - f(\mathbf{x}, \mathbf{y}) * h(\mathbf{x}, \mathbf{y}))}{\partial \mathbf{y}} \sim N(0, \zeta_1)$$

$$\checkmark \frac{\partial^2 (g(\mathbf{x}, \mathbf{y}) - f(\mathbf{x}, \mathbf{y}) * h(\mathbf{x}, \mathbf{y}))}{\partial \mathbf{x}^2} \sim N(0, \zeta_2)$$

$$\checkmark \frac{\partial^2 (g(\mathbf{x}, \mathbf{y}) - f(\mathbf{x}, \mathbf{y}) * h(\mathbf{x}, \mathbf{y}))}{\partial \mathbf{y}^2} \sim N(0, \zeta_2)$$

$$\checkmark \frac{\partial^2 (g(\mathbf{x}, \mathbf{y}) - f(\mathbf{x}, \mathbf{y}) * h(\mathbf{x}, \mathbf{y}))}{\partial \mathbf{x} \partial \mathbf{y}} \sim N(0, \zeta_2)$$

$$\text{SD } \zeta_q = \sqrt{2} \cdot \zeta_{q-1} = \sqrt{2^q} \zeta_0.$$

# Likelihood Model

$$p(g|f, h) \quad \text{Likelihood model}$$

To model the image noise as spatially i.i.d., we combine the constraints signifying that  $\partial^* \mathbf{n}$  with different orders all follow Gaussian distributions, and define the likelihood as

$$p(\mathbf{I}|\mathbf{L}, \mathbf{f}) = \prod_{\partial^* \in \Theta} \prod_i N(\partial^* n_i | 0, \zeta_{\kappa(\partial^*)})$$

$\Theta = \{\partial^0, \partial_x, \partial_y, \partial_{xx}, \partial_{xy}, \partial_{yy}\}$  and define  $\partial^0 n_i = n_i$

# Prior $p(\mathbf{h})$

Since a motion kernel identifies the path of the camera, it tends to be sparse, with most values close to zero.

$$p(\mathbf{h}) = \prod_j e^{-\tau h_j}, h_j \geq 0$$

where  $\tau$  is the rate parameter and  $j$  indexes over elements in the blur kernel.



# Latent Image Prior $p(\mathbf{f})$

We design the latent image prior  $p(\mathbf{f})$  to satisfy two objectives.

- Reduce the ill-posed problem as a regularization
- Reduce ringing artifacts during latent image restoration

$$p(\mathbf{f}) = p_g(\mathbf{f})p_{la}(\mathbf{f})$$

# Latent Image Prior - Global Prior

Natural image gradients tend to follow a heavy-tailed distribution.

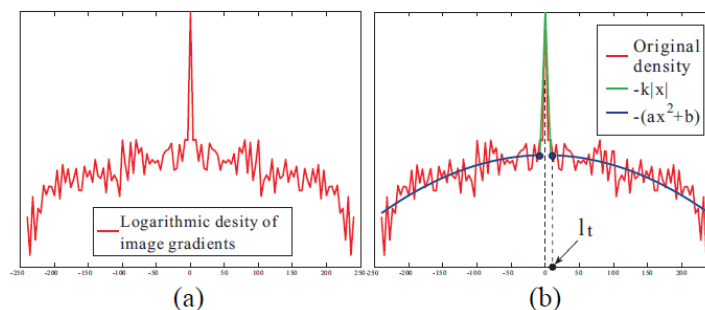


**Figure 7** (a) The curve of the logarithmic density of image gradients. It is computed using information collected from 10 natural images. (b) We construct function  $\Phi(x)$  to approximate the logarithmic density, as shown in green and blue.

Approximate the logarithmic gradient distribution as

$$\Phi(x) = \begin{cases} -k|x| & x \leq l_t \\ -(ax^2 + b) & x > l_t \end{cases}$$

$$p_g(\mathbf{f}) \propto \prod_i e^{\Phi(\partial f_i)} \quad k = 2.7, a = 6.1 \times 10^{-4}, \text{ and } b = 5.0.$$

# Latent Image Prior - Local Prior

**Local prior  $p_l(L)$ .** In this novel prior we use the blurred image to constrain the gradients of the latent image in a fashion that is very effective in suppressing ringing artifacts. This prior is motivated by the fact that motion blur can generally be considered a smooth filtering process. In a locally smooth region of the blurred image, with pixels of almost constant color (as outlined in yellow in Figure 8(a)), the corresponding unblurred image region should also be smooth (as outlined in yellow in Figure 8(b)); that is, its pixels should exhibit no salient edges. Notice that the ringing artifact, as shown in Figure 8(c), usually corresponds to patterned structures and violates this constraint.



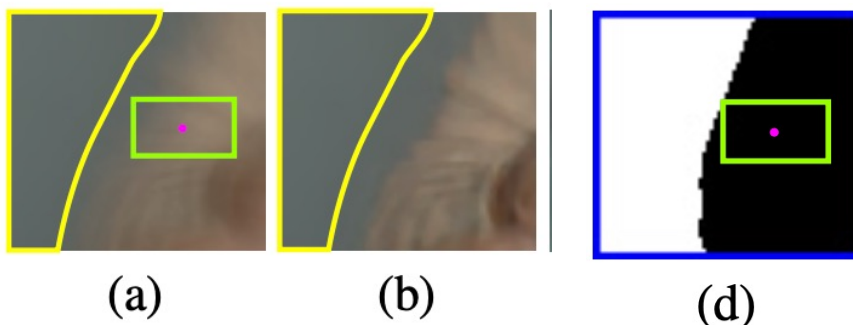
(a) (b)



(c)

# Latent Image Prior - Local Prior

To formulate the local prior, for each pixel  $i$  in blurred image  $I$ , we form a local window with the same size as the blur kernel and centered at it. One example is shown in Figure 8(a) where the window is represented by the green rectangle centered at pixel  $i$  highlighted by the red dot. Then, we compute the standard deviation of pixel colors in each local window. If its value is smaller than a threshold  $t$ , which is set to 5 in our experiments, we regard the center pixel  $i$  as in region  $\Omega$ , i.e.,  $i \in \Omega$ . In Figure 8(d),  $\Omega$  is shown as the set of all white pixels, each of which is at the center of a locally smooth window.



$$p_l(f) = \prod_{i \in \Omega} N\left(\frac{\partial f_i}{\partial x} - \frac{\partial g_i}{\partial x} | 0, \sigma_1\right) N\left(\frac{\partial f_i}{\partial y} - \frac{\partial g_i}{\partial y} | 0, \sigma_1\right)$$

$\Omega$ : the set of pixels with locally smooth neighborhood.

Remark: The value of the standard deviation  $\sigma_1$  is gradually increased over the course of optimization since this prior becomes less important as the blur kernel estimate becomes more accurate.)

# Latent Image Prior - Local Prior

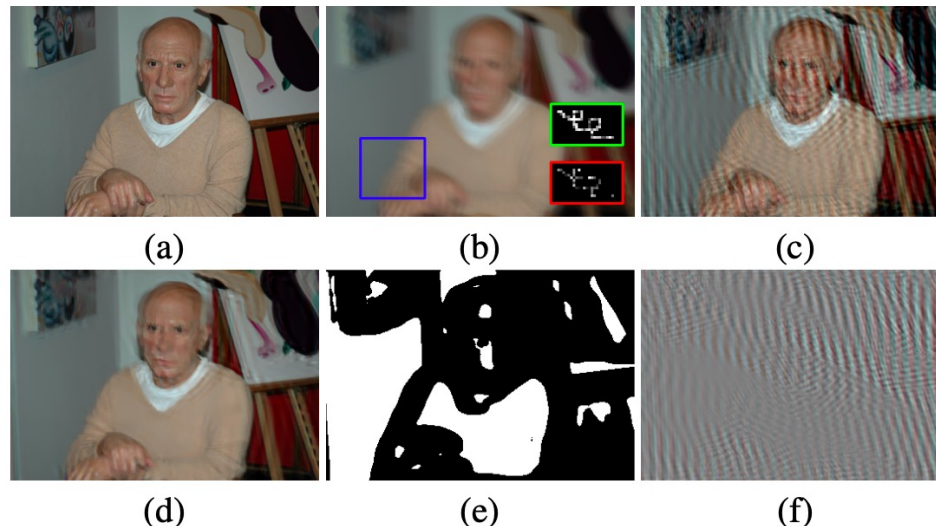
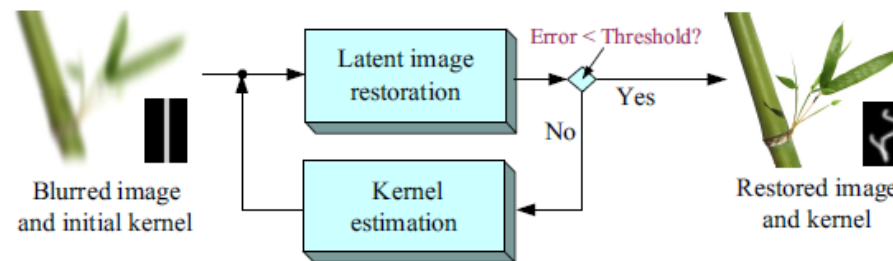


**Figure 9** Effect of prior  $p_l(\mathbf{L})$ . (a) The ground truth latent image. (b) The blurred image. The ground truth blur kernel is shown in the green rectangle. We use the inaccurate kernel in the red frame to restore the blurred image to simulate one image restoration step in our algorithm. (c) The result generated from the image restoration step without using  $p_l(\mathbf{L})$ ; ringing artifacts result. For comparison, we also show our image restoration results in (d) by incorporating  $p_l(\mathbf{L})$ . The computed  $\Omega$  region is shown in white in (e). The ringing map is visualized in (f) by computing the color difference between (c) and (d); the map shows that  $p_l$  is effective in suppressing ringing.

## ➤ Optimization

Minimize the energy function  $E(\mathbf{f}, \mathbf{h}) = -\log(p(\mathbf{f}, \mathbf{h}|\mathbf{g}))$

Optimize E by iteratively estimating  $\mathbf{L}$  and  $\mathbf{f}$ .



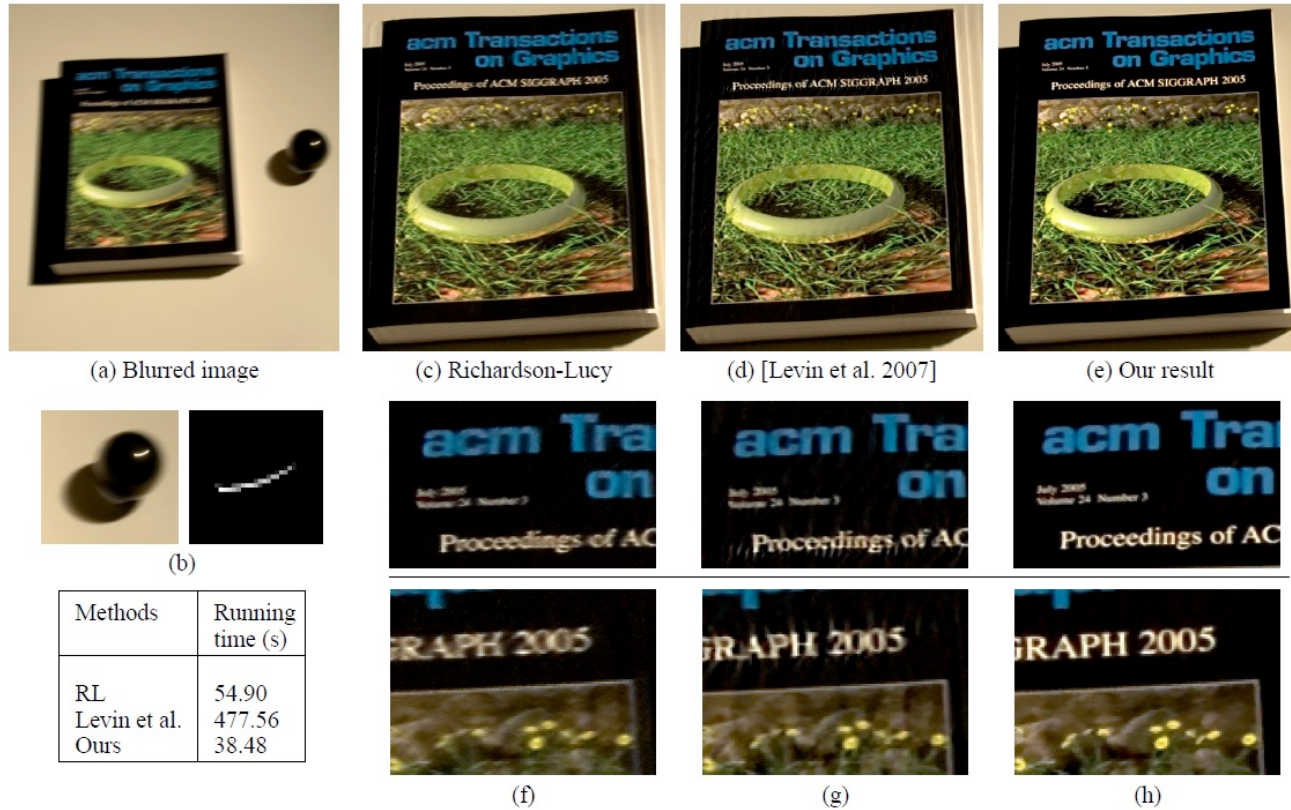


**Figure 12** Non-blind deconvolution. (a) The captured blurry photograph contains a SIGGRAPH proceeding and a sphere for recording the blur PSF. The recovered kernel is shown in (b). Using this kernel, the image restoration methods deconvolve the blurred image and we show in (c) the result of RL algorithm and (d) the result of the sparse prior method [Levin et al. 2007]. Our non-deconvolution result is shown in (e) also using the kernel (b). (f)-(h) Close-ups extracted from (b)-(d), respectively. The running times of different algorithms are also shown.

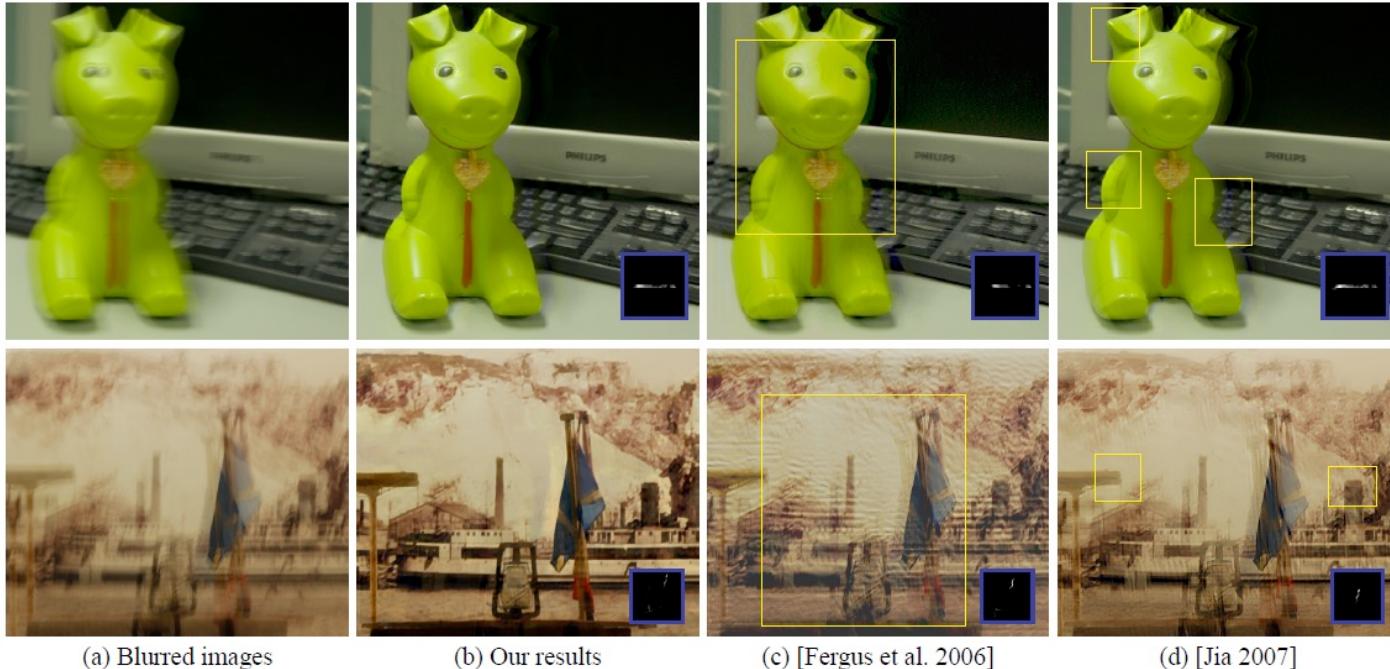


**Figure 13** Blind deconvolution. (a) Our captured blur images. (b) Our results (by estimating both kernels and latent images). The deblurring results of (c) Fergus et al. [2006] and (d) Jia [2007]. The yellow rectangles indicate the selected patches for estimating kernels in (c) and the windows for computing alpha mattes and estimating kernels in (d) respectively. Both Fergus et al. [2006] and Jia [2007] use RL deconvolution to restore the blurred image. The estimated kernels are shown in the blue rectangles.

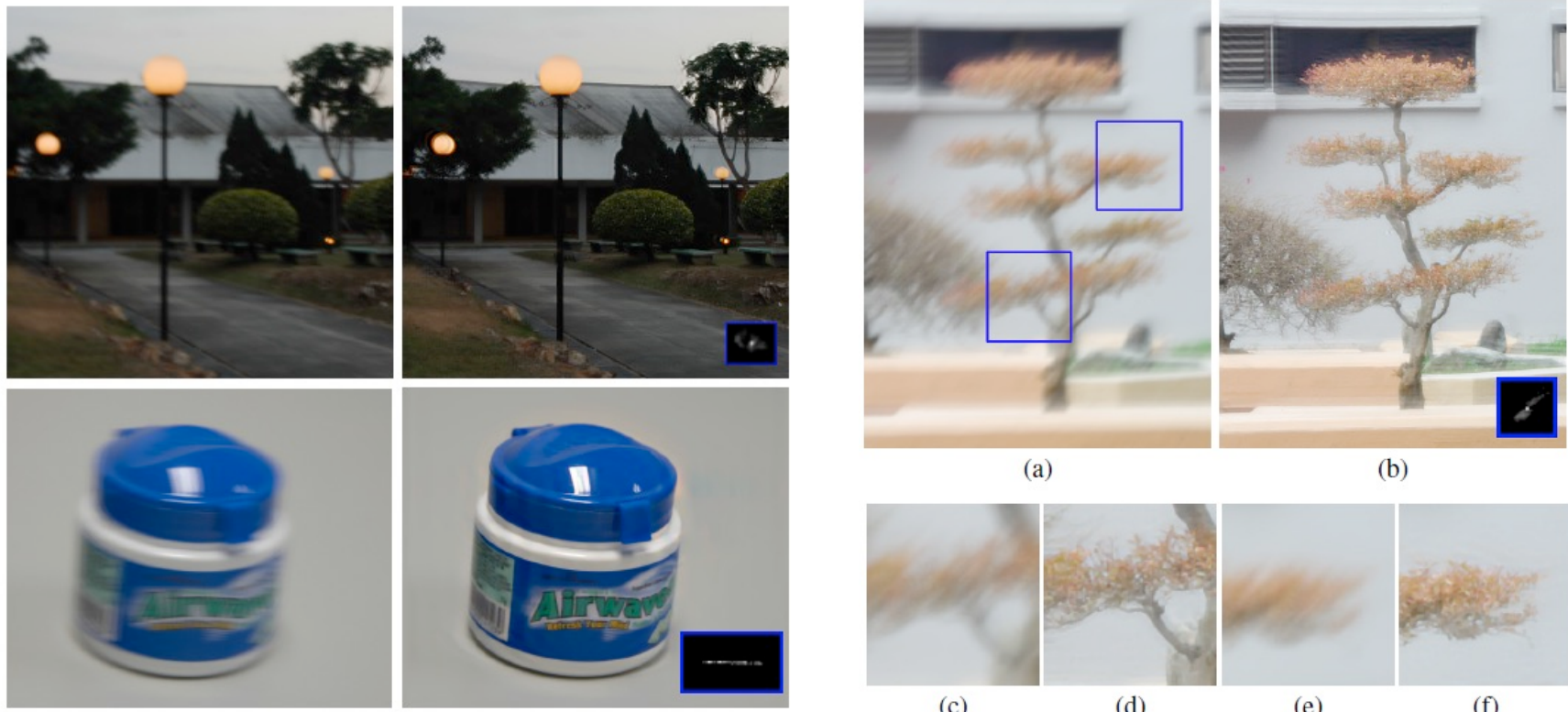


**Figure 16** More results. (a) The captured blur images. (b) Our results. (c)-(f) Close-ups of blurred/unblurred image regions extracted from the last example.